Nonlinear effect of stress and wetting on surface evolution of epitaxial thin films

Yaoyu Pang and Rui Huang
Department of Aerospace Engineering and Engineering Mechanics, University of Texas, Austin, Texas 78712, USA
(Received 11 March 2006; revised manuscript received 20 June 2006; published 10 August 2006)

An epitaxial thin film can undergo surface instability and break up into discrete islands. The stress field and the interface interaction have profound effects on the dynamics of surface evolution. In this work, we develop a nonlinear evolution equation with a second-order approximation for the stress field and a nonlinear wetting potential for the interface. The equation is solved numerically in both two-dimensional (2D) and three-dimensional configurations using a spectral method. The effects of stress and wetting are examined. It is found that the nonlinear stress field alone induces "blow-up" instability, leading to cracklike grooving in 2D and circular pitlike morphology in 3D. For thin films, the blow-up is suppressed by the wetting effect, leading to a thin wetting layer and an array of discrete islands. The dynamics of island formation and coarsening over a large area is well captured by the interplay of the nonlinear stress field and the wetting effect.

DOI: 10.1103/PhysRevB.74.075413 PACS number(s): 81.15.Aa, 81.16.Rf, 68.35.−p, 68.55.−a

I. INTRODUCTION

A macroscopically flat surface of a stressed solid is unstable. The instability is driven by the competition between surface energy and strain energy.[1–3] The rate of surface roughening is controlled by associated kinetics of mass transport, such as surface diffusion. A linear analysis predicts exponential growth of surface perturbation with wavelengths longer than a critical length. Nonlinear analyses in two-dimensional configurations showed that the stress-driven surface instability evolves into a deep, cracklike groove or cusp morphology.[4–8] Experimental investigations have observed similar surface instability and morphology evolution in a number of material systems.[9,10]

An epitaxial thin film is inherently stressed due to lattice mismatch between the film and the substrate, which has drawn tremendous interests for a broad range of applications in electronic and optoelectronic systems.[11] Similar to other stressed solids, the film can undergo surface instability. However, unlike a semi-infinite homogeneous solid, the presence of a substrate affects the instability in several ways. First, the elastic stiffness of the substrate may differ from that of the film, which leads to a different critical wavelength:[12–14] a stiffer substrate tends to stabilize the film and increases the critical wavelength, while the contrary is true for a softer substrate. At the limit of a rigid substrate, a critical film thickness exists, below which the thin film is stable against perturbations of any wavelengths. However, the stiffness effect is insignificant for cases when the film and the substrate have similar elastic properties, such as a SiGe film on a Si substrate.[14] A more important effect is owing to the interface between the film and the substrate. At close proximity to the interface, the wetting interaction between the film and the substrate becomes significant. If the film wets the substrate, the wetting interaction will prevent the substrate from being exposed. Even when the wetting interaction is weak or the film is nonwetting, in which case the substrate surface may be partly exposed, the surface of the unstressed substrate is stable against further roughening. In both cases, instead of forming deep grooves, the film breaks up into discrete islands.[15–18] Furthermore, the mismatch stress in an epitaxial film may also be relaxed by dislocation mechanisms.[17] The competition between surface instability and dislocation mechanisms has been reasonably understood.[19] This paper focuses on diffusion-controlled surface instability and evolution dynamics, assuming dislocation free in the film.

A continuum theory based on nonequilibrium thermodynamics has been developed for modeling surface evolution of epitaxial films. Within this framework, numerical simulations have revealed rich dynamics of surface evolution such as self-assembly of quantum dots.[20–22] However, three-dimensional (3D) nonlinear simulations have been limited to small surface areas or a small number of quantum dots. Some large-scale simulations assumed same elastic properties for the film and the substrate.[21] Alternatively, Spencer *et al.*[23] derived a simple evolution equation in the limit of a rigid substrate and under a small-slope approximation. They found that the solution blows up in a finite time, similar to formation of the cracklike morphology in stressed semi-infinite solids, but with the tip pointing upward (away from the substrate). Golovin *et al.*[24] showed that certain wetting potentials between the film and the substrate can lead to a nonlinear stabilization of the instability and to self-organization of spatially regular arrays of quantum dots or nanopits. Tekalign and Spencer[25] derived a similar evolution equation for a deformable substrate and showed that the equation possesses islandlike steady state solutions in both 2D and 3D. Their equation includes a nonlinear wetting potential and a linear analysis of the stress field. In the present study, we derive a nonlinear evolution equation based on an asymptotic analysis of the stress field including the second-order terms, to study the nonlinear effect of stress in addition to that of wetting. Both 2D and 3D numerical simulations are conducted to study the dynamics of surface evolution. By combining the nonlinear stress analysis with a nonlinear wetting potential, our simulations show island formation over a relatively large area as well as subsequent coarsening and stabilization.

The paper is organized as follows. Section II outlines the general formulation of the model. In Sec. III, an asymptotic analysis of the stress field is presented, following which the linear and nonlinear effects of stress are discussed. Section IV considers the effect of a nonlinear wetting potential, first

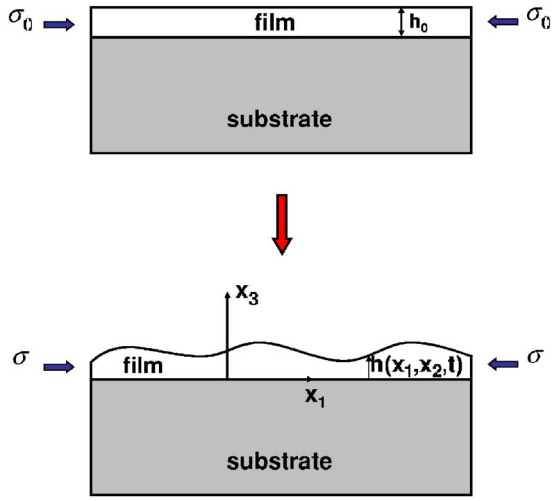

FIG. 1. (Color online) Schematic of surface evolution of an epitaxial film. (a) Reference state. (b) Evolving state.

by a linearized analysis and then by numerical simulations. A spectral method is developed in Secs. III and IV for both 2D and 3D simulations. The results are summarized in Sec. V.

II. GENERAL FORMULATION

Consider an epitaxial thin film on a thick substrate. At the reference state [Fig. 1(a)], the film has a flat surface with a uniform thickness h_0. Due to lattice mismatch between the film and the substrate, the film is subjected to a uniform equibiaxial stress $\sigma_{11}=\sigma_{22}=\sigma_0$. Upon annealing (assuming no deposition), atomic diffusion on the surface leads to evolution of the film surface, with a thickness profile $h(x_1,x_2,t)$, where t is the time of evolution and the coordinates x_j $(j=1,2,3)$ are set up such that $x_3=0$ at the interface between the film and the substrate, as shown in Fig. 1(b). The film is unbounded in the x_1 and x_2 directions. Following the variational analysis by Freund and Jonsdottir,[13] we define a chemical potential at the film surface with respect to the reference plane of a flat surface as

$$\mu(x_1,x_2,t)=\Omega(U_E-\gamma\kappa+U_W)\sqrt{1+h_\alpha h_\alpha}, \tag{1}$$

where U_E represents the elastic strain energy density at the surface, γ is the surface energy density, κ is the surface curvature, U_W represents a wetting potential, $h_\alpha=\frac{\partial h}{\partial x_\alpha}$ $(\alpha=1,2)$ is the gradient of the surface morphology, and Ω is the atomic volume. A repeated Greek subscript implies summation over 1 and 2.

The surface chemical potential, if nonuniform, drives surface diffusion. For simplicity, assume a linear kinetic law, where the diffusion flux is proportional to the gradient of the chemical potential, namely,

$$J_\alpha=-M\frac{\partial\mu}{\partial x_\alpha}, \tag{2}$$

where M represents the mobility of surface atoms. By mass conservation, the divergence of the flux leads to evolution of the thickness profile

$$\frac{\partial h}{\partial t}=\Omega^2 M\frac{\partial^2}{\partial x_\alpha\,\partial x_\alpha}[(U_E-\gamma\kappa+U_W)\sqrt{1+h_\beta h_\beta}]. \tag{3}$$

The evolution equation (3) takes into account the effects of strain energy, surface energy, and wetting energy. Other possible contributions are ignored in the present study.

The elastic strain energy density is given by

$$U_E=\frac{1}{2}\sigma_{ij}\varepsilon_{ij}, \tag{4}$$

where the stress σ_{ij} and the strain ε_{ij} are obtained by solving a boundary value problem of linear elasticity. The subscripts i,j take values 1, 2, and 3; a repeated subscript implies summation over its possible values. Referring to the coordinates in Fig. 1, the boundary condition at the film surface $(x_3=h)$ is

$$\sigma_{ij}n_j=0, \tag{5}$$

with a unit vector of the surface normal given by

$$n_\alpha=\frac{-h_\alpha}{\sqrt{1+h_\beta h_\beta}},\quad n_3=\frac{1}{\sqrt{1+h_\beta h_\beta}}. \tag{6}$$

The interface between the film and the substrate $(x_3=0)$ remains coherent, implying continuity for tractions and displacements. The substrate is assumed to be infinitely thick with both the stress and the displacement diminishing as $x_3\to-\infty$. Due to the nonlinearity in the boundary condition (5), the elasticity problem in general must be solved numerically, which is computationally expensive in 3D. An alternative approach will be developed in Sec. III.

The surface curvature is given by

$$\kappa=\frac{(1+h_\alpha h_\alpha)h_{\beta\beta}-h_\alpha h_\beta h_{\alpha\beta}}{(1+h_\alpha h_\alpha)^{3/2}}. \tag{7}$$

The sign of κ is defined such that it is positive for a concave surface. The curvature can be expanded as

$$\kappa=h_{\beta\beta}\left(1-\frac{1}{2}\delta^2\right)-h_{\alpha\beta}h_\alpha h_\beta+O(\delta^4), \tag{8}$$

where $\delta=\sqrt{h_\alpha h_\alpha}$ is the magnitude of the surface gradient vector. In the present study, only the linear term $(\kappa=h_{\beta\beta})$ is used for the first and second-order analyses, because the first nonlinear term in Eq. (8) is of the third order.

For the wetting potential, we adopt a "transition-layer" model[26] based on a surface energy that depends on the film thickness and undergoes a rapid transition from γ_f (film) to γ_s (substrate) over a length scale b, i.e.,

$$\gamma(h)=\frac{1}{2}(\gamma_f+\gamma_s)+\frac{1}{\pi}(\gamma_f-\gamma_s)\arctan\left(\frac{h}{b}\right). \tag{9}$$

Equation (9) leads to a nonlinear wetting potential

$$U_W=\frac{\gamma_f-\gamma_s}{\sqrt{1+h_\alpha h_\alpha}}\frac{b}{\pi(b^2+h^2)}. \tag{10}$$

The physical significance of the length b and the wetting potential will be discussed in Sec. IV. Other types of wetting potentials[6,27,28] have been proposed, with qualitatively similar effects.

It should be noted that the present formulation assumes an isotropic system, with isotropic elastic properties for the film and the substrate, isotropic surface energy density, isotropic wetting potential, and isotropic surface diffusion mobility. In addition, the surface energy density is assumed to be independent of deformation. More sophisticated models taking into account the effects of anisotropy and strain-dependent surface energy (i.e., surface stress) can be found elsewhere.[29–31] The present study focuses on nonlinear effects of stress and wetting on the evolution dynamics based on the isotropic model.

III. EFFECT OF STRESS

At the reference state [Fig. 1(a)], the strain energy density in the film is uniform, namely,

$$U_E^{(0)} = \frac{1-\nu_f}{E_f}\sigma_0^2, \tag{11}$$

where E_f is Young's modulus of the film and ν_f Poisson's ratio. However, the reference state is an unstable equilibrium configuration because a small perturbation can grow. As the surface evolves, the stress field changes, governed by the boundary condition (5). Following an approach by Xiang and E,[8] we expand the stress into a series in the order of the surface gradient, namely,

$$\sigma_{ij} = \sigma_{ij}^{(0)} + \delta\sigma_{ij}^{(1)} + \delta^2\sigma_{ij}^{(2)} + \cdots, \tag{12}$$

where $\sigma_{ij}^{(0)}$ is the stress at the reference state (uniform, equibiaxial for the present case). The second term on the right-hand side of Eq. (12) represents the linear perturbation to the stress field. The third term is to the second order of the magnitude of the surface gradient, as the leading term of the nonlinear stress field. While higher order terms can be included, the present study will be confined to the second order. In the following, we solve the boundary value problems for the first- and second-order stresses, respectively, from which the first- and second-order strain energy terms are determined. The surface evolution equation (3) is then solved analytically and numerically. To focus on the stress effect, the wetting potential is not included in this section.

A. First-order solution: Linear analysis

Substituting Eq. (12) into (5) and keeping only the first-order terms, we obtain the boundary condition for the first-order stress field

$$\delta\sigma_{3\alpha}^{(1)} = \sigma_0 h_\alpha \quad \text{and} \quad \delta\sigma_{33}^{(1)} = 0. \tag{13}$$

The stress field in general depends on the elastic properties of both the film and the substrate. At the limit of a thin film, however, the deformation is predominantly controlled by the elastic substrate.[14] In this case, the corresponding surface displacement of the film can be approximately obtained by applying the surface traction onto the surface of the semi-infinite substrate. From the solution to the classical Cerruti's problem in linear elasticity, a simple form of the surface displacement is obtained in terms of Fourier transforms

$$\hat{u}_\alpha^{(1)} = ik_\beta C_{\alpha\beta}\sigma_0\hat{h}, \tag{14}$$

where $\hat{u}_\alpha^{(1)}$ and $\hat{h}$ are the Fourier transforms of the surface displacement and the thickness profile, respectively, $C_{\alpha\beta}$ is the compliance matrix of the substrate given in the Appendix, Eq. (A2), and k_β is the component of the wave vector in the Fourier space. The thin-film approximation effectively takes into account the elastic properties of the substrate, while the mismatch stress σ_0 depends on the elastic properties of the film. Consequently, different elastic properties can be accommodated. Equation (14) is exact if the film and the substrate have identical elastic properties, thus can also be used as a reasonable approximation for cases with elastically similar film and substrate materials.

Corresponding to the surface displacement in Eq. (14), the first-order elastic strain energy density at the surface is

$$U_E^{(1)} = \sigma_0\frac{\partial u_\alpha^{(1)}}{\partial x_\alpha}. \tag{15}$$

Substituting Eq. (15) into the evolution equation (3) and again keeping the first-order terms only, we obtain the first-order evolution equation

$$\frac{\partial h}{\partial t} = \Omega^2 M\frac{\partial^2}{\partial x_\beta \partial x_\beta}\left(\sigma_0\frac{\partial u_\alpha^{(1)}}{\partial x_\alpha} - \gamma_f h_{\alpha\alpha}\right). \tag{16}$$

Fourier transform of Eq. (16) leads to

$$\frac{\partial \hat{h}}{\partial t} = \Omega^2 M k^2\left(\frac{2\sigma_0^2}{\bar{E}_s}k - \gamma_f k^2\right)\hat{h}, \tag{17}$$

where $\bar{E}_S = \frac{E_S}{1-\nu_S^2}$ is the plane-strain modulus of the substrate and $k^2 = k_1^2 + k_2^2$.

The two terms in the bracket of Eq. (17) compete: the first term, strain energy, drives surface instability, while the second term, surface energy, stabilizes the surface. The competition sets up a length scale and an associated time scale, namely,

$$L = \frac{\gamma_f \bar{E}_s}{2\sigma_0^2}, \tag{18}$$

$$\tau = \frac{L^4}{\Omega^2 M\gamma_f} = \frac{\gamma_f^3 \bar{E}_s^4}{16\Omega^2 M\sigma_0^8}. \tag{19}$$

For a constant wave number k, the solution to Eq. (17) is simply

$$\hat{h}(k,t) = A\exp\left(\frac{st}{\tau}\right), \tag{20}$$

where $s = (kL)^3(1-kL)$ is the normalized growth rate. A critical wavelength ($\lambda_c = 2\pi L$) and the fastest growing mode ($\lambda_m = \frac{8}{3}\pi L$) can be determined accordingly. This result agrees with previous studies by linear perturbation analysis.[12–14]

To simulate surface evolution with an arbitrary initial perturbation, a spectral method is employed for numerical simulations. At each step, the current thickness profile is transformed into the Fourier space by fast Fourier transform

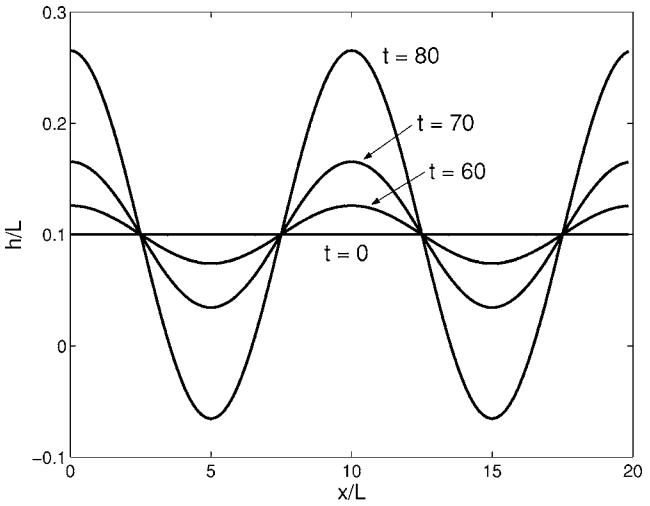

FIG. 2. Two-dimensional simulation of surface evolution based on the linear analysis.

(FFT). The evolution equation (17) is integrated by a backward Euler scheme of finite difference

$$\hat{h}^{(n+1)} = \frac{\hat{h}^{(n)}}{1 - s\Delta t}, \tag{21}$$

where Δt is the time step, normalized by the time scale in Eq. (19). The new profile can then be obtained by an inverse FFT, assuming periodic boundary conditions in the plane of the film. Same procedure can be applied for both 2D and 3D configurations. Notably, normalization with the length L and the time τ leads to a generic equation with no system-specific parameters. Consequently, numerical simulations can be performed without specifying any particular material properties; the result is general for all systems in the linear regime, with the system dependence implicitly accounted for by the definitions of the length and time scales.

The result from a 2D simulation is shown in Fig. 2, where the film thickness varies in one direction only. A film stripe of $20L$ width is considered, whose surface is discretized into 128 grid points. The simulation starts from a sinusoidal perturbation with a wavelength $10L$ (close to the fastest growing mode) and a small amplitude ($10^{-4}L$), using the normalized time step $\Delta t=0.1$. As the amplitude of the perturbation grows, the surface profile remains sinusoidal, as expected from the linear perturbation analysis. Figure 3 shows the result from a 3D simulation, with a square computational cell of size $100L$ by $100L$, starting from a random initial perturbation [Fig. 3(a)]. The computational cell is discretized into a 128 by 128 grid, and the normalized time step is again 0.1. Refining the computational grid and the time step leads to no difference in the simulation results. As shown in Figs. 3(b)–3(e), the surface pattern quickly selects a characteristic length. Subsequently, the overall pattern remains unchanged, while the root mean square (r.m.s) roughness of the surface grows. Therefore, using the first-order evolution equation, the film surface evolves self-similarly in both 2D and 3D configurations. The Fourier spectrum of the surface pattern [Fig. 3(f)] exhibits a circular ring of the peak intensity at the radius corresponding to the wave number of the fastest growing mode $2\pi L/\lambda_m=0.75$. The randomly oriented labyrinth-type surface pattern is a common feature for isotropic systems, similar to the domain patterns of modulated phases in a variety of physical-chemical systems[32] and the wrinkling patterns of thin films.[33,34]

B. Second-order analysis: Nonlinear effect of stress

Following the same procedure as in the previous section, the second-order terms in the nonlinear boundary condition (5) lead to

$$\delta^2\sigma_{3\alpha}^{(2)} = \delta\sigma_{\alpha\beta}^{(1)}h_\beta \quad \text{and} \quad \delta^2\sigma_{33}^{(2)} = \sigma_0 h_\beta h_\beta. \tag{22}$$

Here both shear and normal tractions are in action for the second-order field. Under the thin-film approximation described earlier, the Fourier transform of the second-order surface displacement is

$$\hat{u}_\alpha^{(2)} = C_{\alpha\beta}\hat{\varphi}_\beta + C_{\alpha 3}\sigma_0\hat{\phi}, \tag{23}$$

where $\varphi_\beta=\delta\sigma_{\beta\gamma}^{(1)}h_\gamma$, $\phi=h_\beta h_\beta$, and the elastic compliances C_{ij} are given in Eq. (A2). The corresponding second-order strain energy density at the surface is

$$U_E^{(2)} = \frac{1}{2}\delta\sigma_{ij}^{(1)}\varepsilon_{ij}^{(1)} + \sigma_0\frac{\partial u_\alpha^{(2)}}{\partial x_\alpha}. \tag{24}$$

Noting Eq. (13) for the first-order surface tractions, the first term at the right-hand side of Eq. (24) can be written as

$$\frac{1}{2}\delta\sigma_{ij}^{(1)}\varepsilon_{ij}^{(1)} = \frac{1+\nu_f}{1-\nu_f}U_E^{(0)}\phi + \psi, \tag{25}$$

where $\psi=\frac{1}{2}\delta\sigma_{\alpha\beta}^{(1)}\varepsilon_{\alpha\beta}^{(1)}$ and

$$\varepsilon_{\alpha\beta}^{(1)} = \frac{1}{2}\left(\frac{\partial u_\alpha^{(1)}}{\partial x_\beta} + \frac{\partial u_\beta^{(1)}}{\partial x_\alpha}\right), \tag{26}$$

$$\delta\sigma_{\alpha\beta}^{(1)} = \frac{E_f}{1+\nu_f}\left(\varepsilon_{\alpha\beta}^{(1)} + \frac{\nu_f}{1-\nu_f}\varepsilon_{\gamma\gamma}^{(1)}\delta_{\alpha\beta}\right). \tag{27}$$

Substituting Eq. (25) into Eq. (24) and then into Eq. (3), together with the zero and first-order strain energies in Eqs. (11) and (15), and keeping terms up to the second order, we obtain a nonlinear evolution equation

$$\frac{\partial h}{\partial t} = \Omega^2 M\frac{\partial^2}{\partial x_\beta \partial x_\beta}\left(\sigma_0\frac{\partial u_\alpha^{(1)}}{\partial x_\alpha} - \gamma_f h_{\alpha\alpha} + \sigma_0\frac{\partial u_\alpha^{(2)}}{\partial x_\alpha} + \frac{3+\nu_f}{2(1-\nu_f)}U_E^{(0)}\phi + \psi\right). \tag{28}$$

The first two terms in the bracket of Eq. (28) are the linear terms as in the first-order equation (16), and the last three terms are the nonlinear terms of second order.

Fourier transform of Eq. (28) leads to

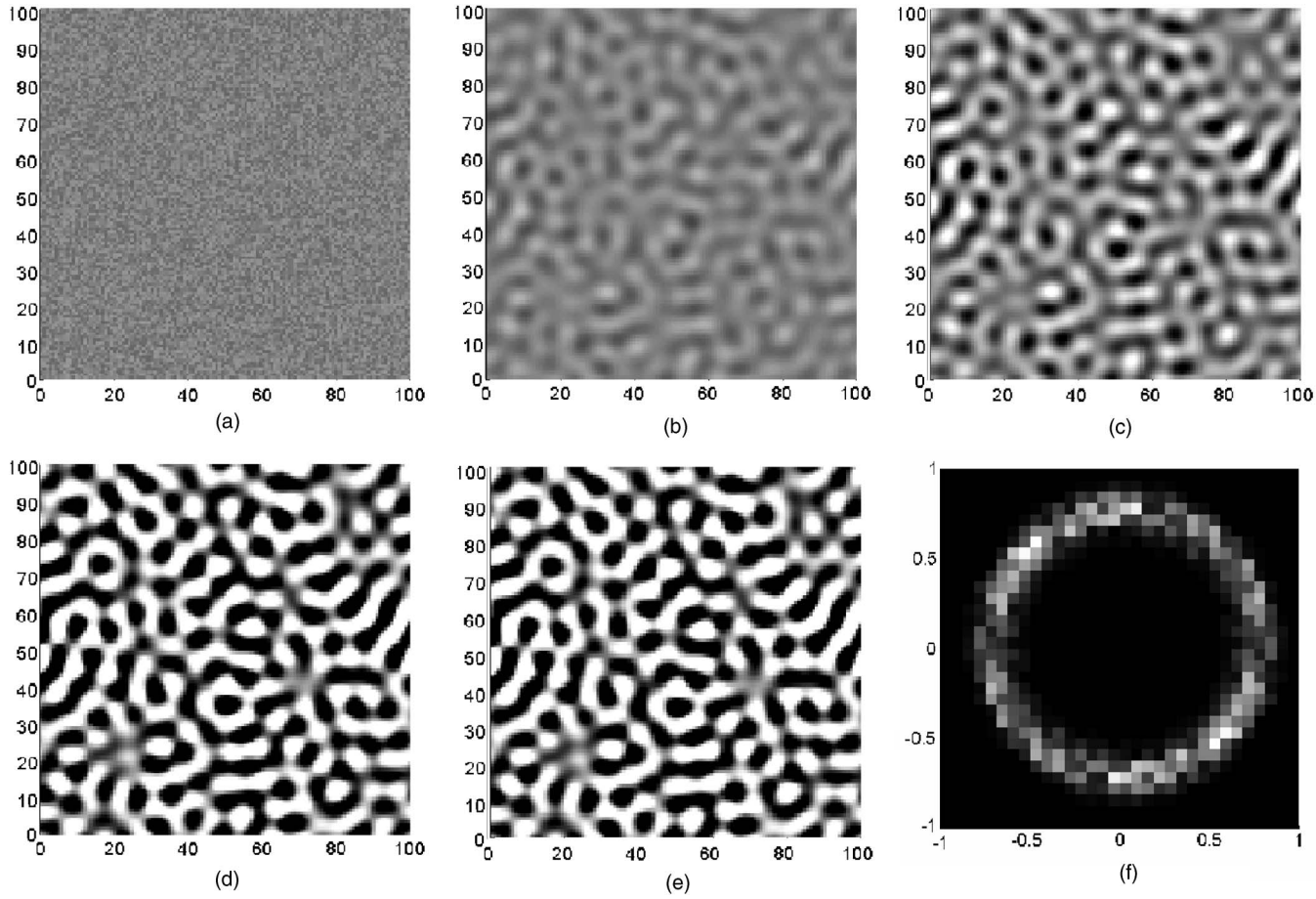

FIG. 3. Three-dimensional simulation of surface evolution based on the linear analysis. (a)–(e) are gray scale contour plots of the thickness profile $h(x_1,x_2)$, white for crests and dark for troughs. (a) Random perturbation at $t=0$, r.m.s. $=5.77\times10^{-5}$; (b) $t=20$, r.m.s. $=7.40\times10^{-5}$; (c) $t=50$, r.m.s. $=1.64\times10^{-3}$; (d) $t=75$, r.m.s. $=2.39\times10^{-2}$; (e) $t=100$, r.m.s. $=3.60\times10^{-1}$; (f) the Fourier spectrum of the surface pattern, which remains the same for (b)–(e).

$$\frac{\partial \hat{h}}{\partial t} = \Omega^2 M k^2 \left[\left(\frac{2\sigma_0^2}{\bar{E}_s} k - \gamma_f k^2 \right) \hat{h} - ik_\alpha C_{\alpha\beta} \hat{\varphi}_\beta \sigma_0 - A U_E^{(0)} \hat{\phi} - \hat{\psi} \right], \tag{29}$$

where

$$A = \frac{3+\nu_f}{2(1-\nu_f)} + \frac{(1+\nu_f)(1-2\nu_s)}{1-\nu_s} \frac{\bar{E}_f}{\bar{E}_s}. \tag{30}$$

A semi-implicit algorithm is adopted to integrate Eq. (29), where the linear part is integrated by a backward finite difference scheme and the nonlinear part by a forward scheme. The time integration takes the form

$$\hat{h}^{(n+1)} = \frac{\hat{h}^{(n)} - Q^{(n)} \Delta t}{1 - s\Delta t}, \tag{31}$$

where s is the normalized growth rate as obtained from the linear analysis and

$$Q = \frac{1}{2} k^2 \left[\frac{A\bar{E}_s}{(1+\nu_f)\bar{E}_f} \hat{\phi} + \frac{\bar{E}_s}{\bar{E}_f \bar{\sigma}_0^2} \hat{\psi} + \frac{1}{\bar{\sigma}_0} ik_\alpha \bar{C}_{\alpha\beta} \hat{\varphi}_\beta \right]. \tag{32}$$

The length scale L, the time scale τ, and the modulus $\bar{E}_f$ have been used above to normalize length, time, and stress, respectively. Unlike the first-order equation, numerical simulation of the second-order equation requires specification of a set of physical parameters, including the normalized mismatch stress ($\bar{\sigma}_0=\sigma_0/\bar{E}_f$), the modulus ratio ($\bar{E}_s/\bar{E}_f$), and the Poisson's ratios (ν_f and ν_s).

A brief description of the numerical procedures follows. Starting with a thickness profile $h(x_1,x_2,t)$, compute $\hat{h}(k_1,k_2,t)$ with the fast Fourier transform (FFT). Then, in the Fourier space, compute $ik_\alpha \hat{h}$, $\hat{u}_\alpha^{(1)} = ik_\beta C_{\alpha\beta} \hat{h}\sigma_0$, and $ik_\beta \hat{u}_{\alpha_{(1)}}^{(1)}$, by simple multiplications. Next, we obtain h_α, $u_\alpha^{(1)}$, and $\frac{\partial u_{\alpha_{(1)}}}{\partial x_\beta}$ by inverse FFT, and compute the nonlinear terms $\phi = h_\alpha h_\alpha$, $\varphi_\alpha = \delta\sigma_{\alpha\beta}^{(1)} h_\beta$, and $\psi = \frac{1}{2}\delta\sigma_{\alpha\beta}^{(1)} \epsilon_{\alpha\beta}^{(1)}$, in the real space, again by simple multiplications at each grid point. After transforming the nonlinear terms into the Fourier space, Eq. (31) is used to update the Fourier transform of the thickness profile $\hat{h}(k_1,k_2,t+\Delta t)$. The new thickness profile is then obtained by

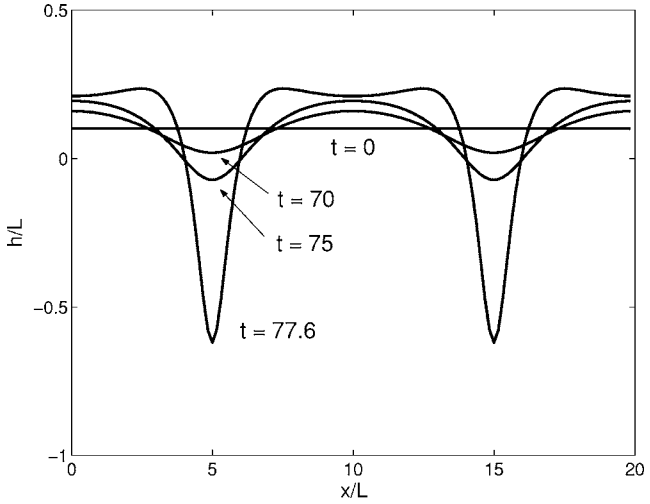

FIG. 4. Two-dimensional simulation of surface evolution by the nonlinear analysis with no wetting effect.

an inverse FFT. The procedures repeat to simulate evolution of the thickness profile. Similar numerical methods have been used in simulations of other evolution problems[35,36] with good stability and efficiency.

The result from a 2D simulation is shown in Fig. 4. The normalized physical parameters are $\bar{\sigma}_0=0.01$, $\bar{E}_f/\bar{E}_s=1.1$, and $\nu_f=\nu_s=0.25$. All the numerical parameters are identical to those in Fig. 2, and the convergence of the result was confirmed with finer discretization and time steps. The result is dramatically different from Fig. 2. Instead of self-similar evolution of a sinusoidal perturbation, the surface develops deep grooves, exemplifying the effect of the nonlinear stress field. The result is similar to those obtained by Spencer and Meiron[7] and Xiang and E,[8] but different from that by Yang and Srolovitz.[4,5] In the latter case, the grooving was more localized, which may be attributed to stronger nonlinearity in the finite element model as opposed to the second-order consideration in the present study. As pointed out by Yang and Srolovitz,[4,5] the grooving may lead to nucleation of surface cracks in a stressed solid, even with an initially defect-free, nearly flat surface. For an epitaxial thin film on a substrate, however, the development of deep grooving would be suppressed by the wetting effect at the film/substrate interface, as will be discussed in Sec. IV.

A 3D simulation is shown in Fig. 5, with the same physical parameters as for Fig. 4. The numerical parameters (including the initial random perturbation) are identical to those in Fig. 3. The initial stage of surface evolution is similar to Fig. 3. However, after a finite time, the solution blows up [Figs. 5(e) and 5(f)]. Instead of a cracklike grooving expected from the 2D simulations,[4–8] the surface develops a circular pitlike morphology. The result persists with finer nu-

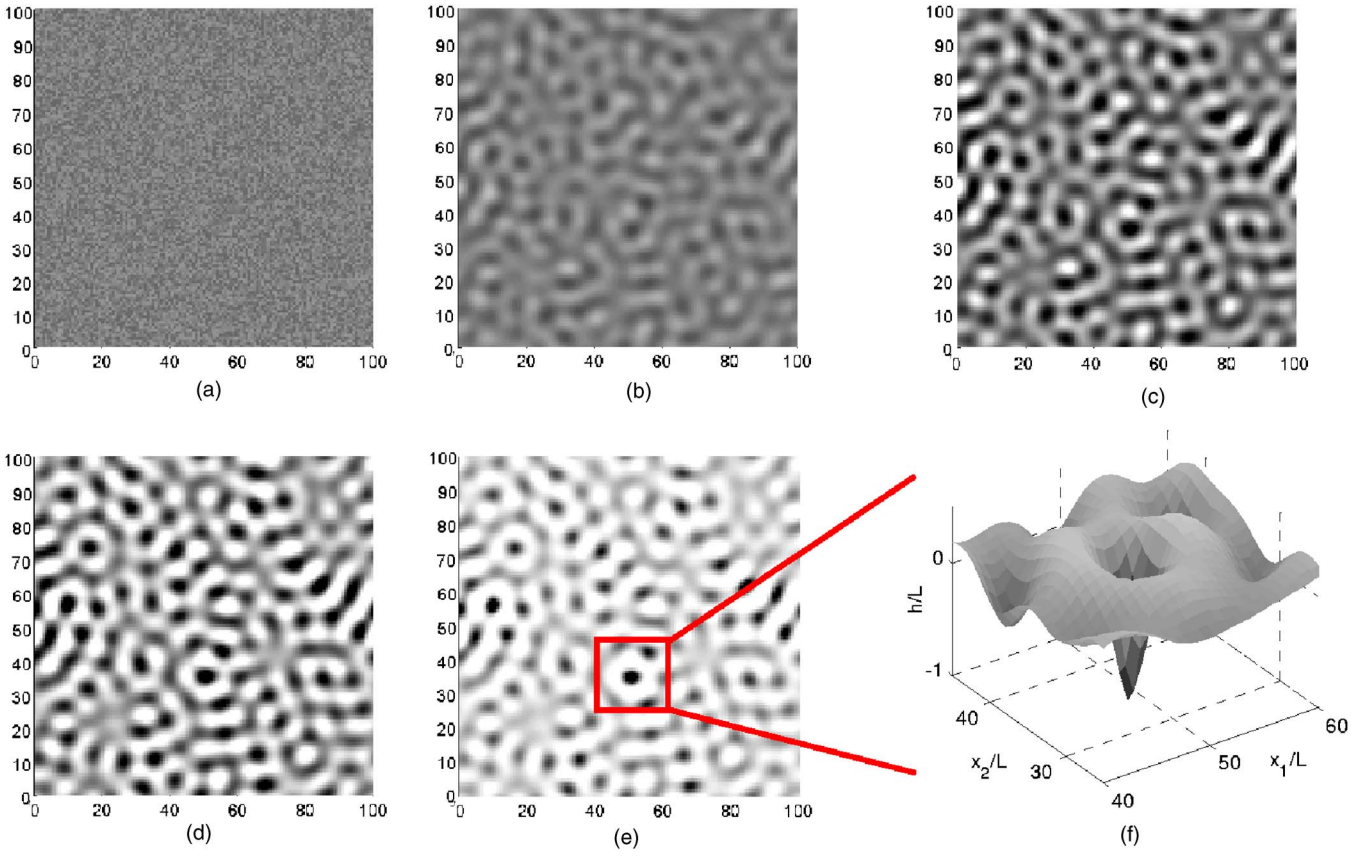

FIG. 5. (Color online) Three-dimensional simulation of surface evolution based on the nonlinear analysis with no wetting effect. (a)–(e) are gray scale contour plots of the thickness profile $h(x_1,x_2)$, white for crests and dark for troughs. (a) Random perturbation at $t=0$, r.m.s. $=5.77\times10^{-5}$; (b) $t=20$, r.m.s. $=7.40\times10^{-5}$; (c) $t=50$, r.m.s. $=1.64\times10^{-3}$; (d) $t=75$, r.m.s. $=2.44\times10^{-2}$; (e) $t=88$, r.m.s. $=1.24\times10^{-1}$; (f) the local 3D view of a circular pit at $t=88$.

merical grids and time steps. Similar features were also observed in previous studies.[24] This is believed to be a result of the isotropic model, where both the driving force and the kinetics are isotropic, with no particular direction(s) favored for grooving. On the other hand, the cracklike morphology observed in experiments could be due to the effect of anisotropy in the real systems. For example, in one case, the applied stress was uniaxial.[10] Furthermore, even for an isotropic system, it has been known that a circular void in a stressed solid can be unstable and evolve into a cracklike slit.[37] This process, however, is not captured in the present model because the simulation becomes numerically unstable shortly after the blow up: the tip of the circular pit advances increasingly faster, requiring higher-order nonlinear analysis for simulations of further evolution.

The above numerical simulations clearly demonstrate the effect of the nonlinear stress field on the dynamics of surface evolution. The nonlinear behavior is far from what can be expected from a linear analysis, and the results can be quite different between 2D and 3D configurations. Since the wetting potential is ignored, the effect of the film/substrate interface is not accounted for and the result is essentially identical to that for stressed semi-infinite solids. For thin films, however, the wetting effect must be considered explicitly, as discussed in the next section.

IV. EFFECT OF WETTING

The transition-layer model[26] assumes a smooth transition of the surface energy density and leads to a self-consistent wetting potential as given in Eq. (10). The effect of this wetting potential on surface evolution is discussed in this section.

A. Linear analysis of wetting effect

In the same spirit of the linear analysis of the stress effect, by linearizing the wetting potential in Eq. (10), we obtain the first-order evolution equation with the wetting effect

$$\frac{\partial h}{\partial t} = \Omega^2 M \frac{\partial^2}{\partial x_\beta \partial x_\beta}\left(\sigma_0 \frac{\partial u_\alpha^{(1)}}{\partial x_\alpha} - \gamma_f h_{\alpha\alpha} - \frac{2(\gamma_f - \gamma_s)b}{\pi h_0^3} h\right). \tag{33}$$

Fourier transform of Eq. (33) leads to

$$\frac{\partial \hat{h}}{\partial t} = \Omega^2 M k^2 \left(\frac{2\sigma_0^2}{\bar{E}_s} k - \gamma_f k^2 + \frac{2b(\gamma_f - \gamma_s)}{\pi h_0^3}\right)\hat{h}. \tag{34}$$

For a constant wave number k, the solution to Eq. (34) takes the same form as Eq. (20), but with a different growth rate

$$s = (kL)^2\left[kL - (kL)^2 + \frac{2bL^2(\gamma_f - \gamma_s)}{\pi h_0^3 \gamma_f}\right]. \tag{35}$$

The third term in the bracket of Eq. (35) represents the effect of wetting on the initial growth rate, which depends on the film thickness (h_0) and the transition of surface energy (i.e., γ_s, γ_f, b). The growth rate versus the wave number is plotted in Fig. 6 for different film thicknesses. When $\gamma_f < \gamma_s$, a critical thickness is defined as

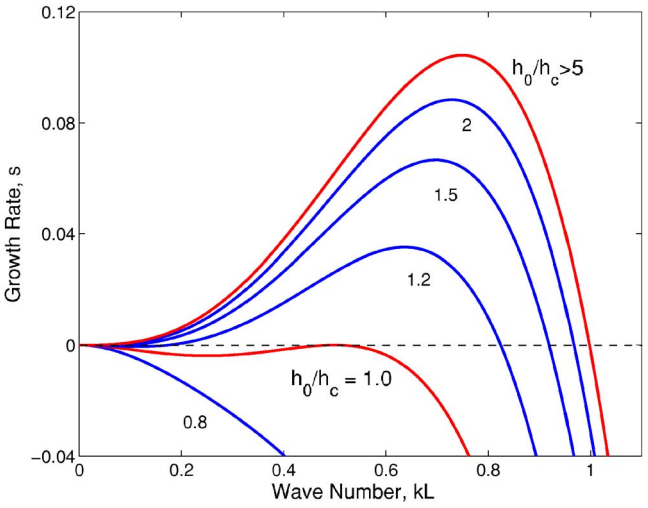

FIG. 6. (Color online) Linear analysis of the wetting effect: the growth rate versus the wave number for different film thickness. The critical thickness h_c is defined by Eq. (36).

$$h_c = 2L\left(\frac{b(\gamma_s - \gamma_f)}{\pi L \gamma_f}\right)^{1/3}. \tag{36}$$

If $h_0 < h_c$, the growth rate is negative for all wave numbers; the film is thus stable with a flat surface. If $h_0 > h_c$, the growth rate becomes positive for wave numbers between two critical values. Consequently the flat surface becomes unstable. This is consistent with the Stranski-Krastanov growth of epitaxial thin films, in which the film morphology undergoes a 2D-3D transition after a critical thickness.[15] Using typical values $\sigma_0 = 1$ GPa, $\bar{E}_s = 150$ GPa, $\gamma_f = 1$ N/m, $\gamma_s = 1.2$ N/m, and $b = 0.1$ nm, we obtain that $h_c = 6.6$ nm, in reasonable agreement with experimental observations. The critical thickness weakly depends on the length b, which may be selected empirically. For relatively thick films (e.g., $h_0 > 5h_c$), the wetting effect is negligible at the initial stage, and the growth rate is essentially independent of the film thickness. In between, both the growth rate and the fastest growing wave number increases as the film thickness increases. The wetting potential therefore has a significant effect on surface stability and evolution of thin films ($h_0 < 5h_c$).

Interestingly, if $\gamma_f > \gamma_s$, the present analysis predicts that the film becomes increasingly unstable as the thickness decreases. Consequently, the film tends to form clusters at the beginning of growth, characteristic of the Volmer-Weber mode.[38] The dynamics of surface evolution for this case will be left for future studies.

B. Nonlinear effect of wetting

Including the full nonlinear wetting potential, Eq. (10) together with the second-order stress field, leads to a nonlinear evolution equation

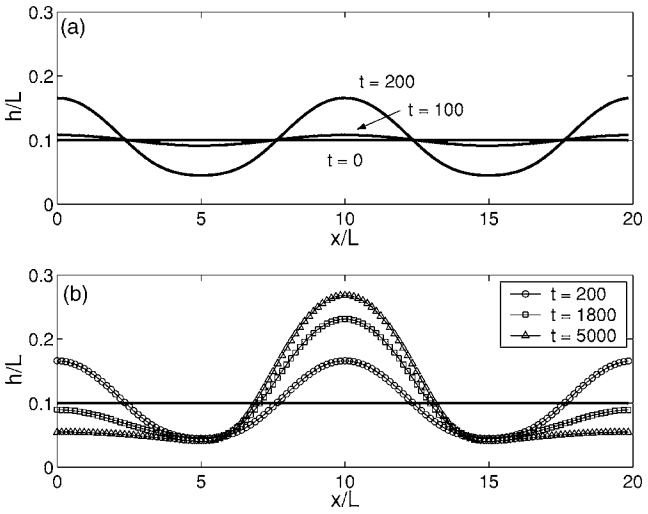

FIG. 7. Two-dimensional simulation of surface evolution based on the nonlinear analysis of both stress and wetting effect: (a) stable growth $(0<t<200)$; (b) coarsening $(t>200)$.

$$\frac{\partial h}{\partial t} = M\Omega^2 \frac{\partial^2}{\partial x_\beta \partial x_\beta}\left[\sigma_0 \frac{\partial u_\alpha^{(1)}}{\partial x_\alpha} - \gamma_f h_{\alpha\alpha} + \sigma_0 \frac{\partial u_\alpha^{(2)}}{\partial x_\alpha} + \frac{3+\nu_f}{2(1-\nu_f)} U_E^{(0)} \phi + \psi - \frac{\gamma_s - \gamma_f}{\pi}\left(\xi h_{\alpha\alpha} + \frac{b}{b^2+h^2}\right)\right], \tag{37}$$

where $\xi = \frac{\pi}{2} - \arctan\left(\frac{h}{b}\right)$.

Following the same procedures described in Sec. III B, numerical simulations of surface evolution are conducted using the spectral method. First, the result from a 2D simulation is shown in Fig. 7. In addition to the same parameters used in Fig. 4, we take $h_0=0.1L$, $b=0.001L$, and $\gamma_s/\gamma_f=1.2$, which leads to a critical thickness $h_c=0.08L$. Starting from a sinusoidal perturbation of wavelength $10L$, the initial stage of surface evolution $(t<100)$ is similar to those in Figs. 2 and 4, but with a slower growth rate due to the wetting effect, as predicted by the linear analysis. Further evolution $(t=200)$ shows stabilization of a wetting layer between the peaks (or islands), differing from the deep grooving morphology observed in Fig. 4. Evidently, the wetting effect prevents exposure of the substrate surface. This result is consistent with the "steady state" predicted by Tekalign and Spencer[25] using the same wetting potential but with a first-order stress analysis. The effect of the nonlinear stress field in the present study becomes prominent as the evolution continues [Fig. 7(b)]. After a long-time, one island grows at the expense of the other. Eventually, only one island remains within the computational domain, resembling the coarsening process observed in experiments,[39] where the number of islands decreases over time. The present simulation shows that the height of the surviving island increases while its lateral size (diameter) and location remain unchanged. This, however, contradicts with experiments where islands typically grow in both height and diameter. The contradiction may be attributed to the effect of anisotropy in the surface energy of real materials, which tends to select a particular surface orientation, thus leading to simultaneous growth in the height and diameter during coarsening as well as shape transition in the later stage.[39] With the isotropic model of the present study, however, more elastic energy can be released as the aspect ratio of the island increases, without much penalty of increasing the surface energy. The effect of anisotropy in the nonlinear analysis will be left for future studies.

Figure 8 shows a 3D simulation of the surface evolution. The computational parameters are the same as in Figs. 3 and 5, including the initial perturbation, the computational grid, and the time step. In addition, as for the 2D simulation in Fig. 7, we take $h_0=0.1L$, $b=0.001L$, and $\gamma_s/\gamma_f=1.2$. The simulation shows similar surface roughening at the initial stage. As predicted by the linear analysis (Fig. 6), the wetting effect leads to a slower growth rate and a longer wavelength for the fastest growing mode. The surface pattern is different owing to the different wavelength. Remarkably, the solution does not blow up, even after a very long time (up to $t=30\,000$). Instead of deep, circular pits in Fig. 5, the film breaks up, forming discrete islands on a thin wetting layer. As observed in the 2D simulation, the wetting effect prevents exposure of substrate surface and leads to self-assembly of an array of islands. Further evolution observes coarsening of the island array: some islands grow higher at the expense of the others; consequently, the island number density decreases over time, in agreement with experimental observations.[39] After a long time of evolution (up to $t=30\,000$), the island array appears to reach an equilibrium state with no further coarsening. However, theoretical proof of the equilibrium state (with minimum total energy) is challenging due to the formidably large number of variables including island size, island shape and spatial organization, and is not available for the 3D configuration. The island size in the final array is quite uniform, but no particular ordering is observed in the spatial pattern. It is noted that, while island coarsening is generally observed in experiments, it is not a ubiquitous feature. In a growth regime very close to the thermodynamic equilibrium, such as liquid phase epitaxy reported by Dorsch *et al.*,[40] coarsening was not observed. In spite of the limitations of the present model, the dynamics of island formation and coarsening over a large area is reasonably captured by the interplay of the nonlinear stress field and the wetting effect.

Figure 9 compares the evolution of the surface roughness obtained from the 3D simulations (i.e., Figs. 3, 5, and 8). The surface roughness is quantitatively determined by the root mean square (r.m.s.) of the thickness profile, namely,

$$\text{r.m.s.}(t) = \sqrt{\frac{1}{N^2}\sum_{m=1}^{N}\sum_{n=1}^{N}[h(m,n,t)-h_0]^2}, \tag{38}$$

where $N=128$ is the number of the grid points along one side of the computational cell, and $h(m,n,t)$ is the local thickness at the grid point (m,n). Without the wetting effect, the surface roughness initially grows exponentially, with the same

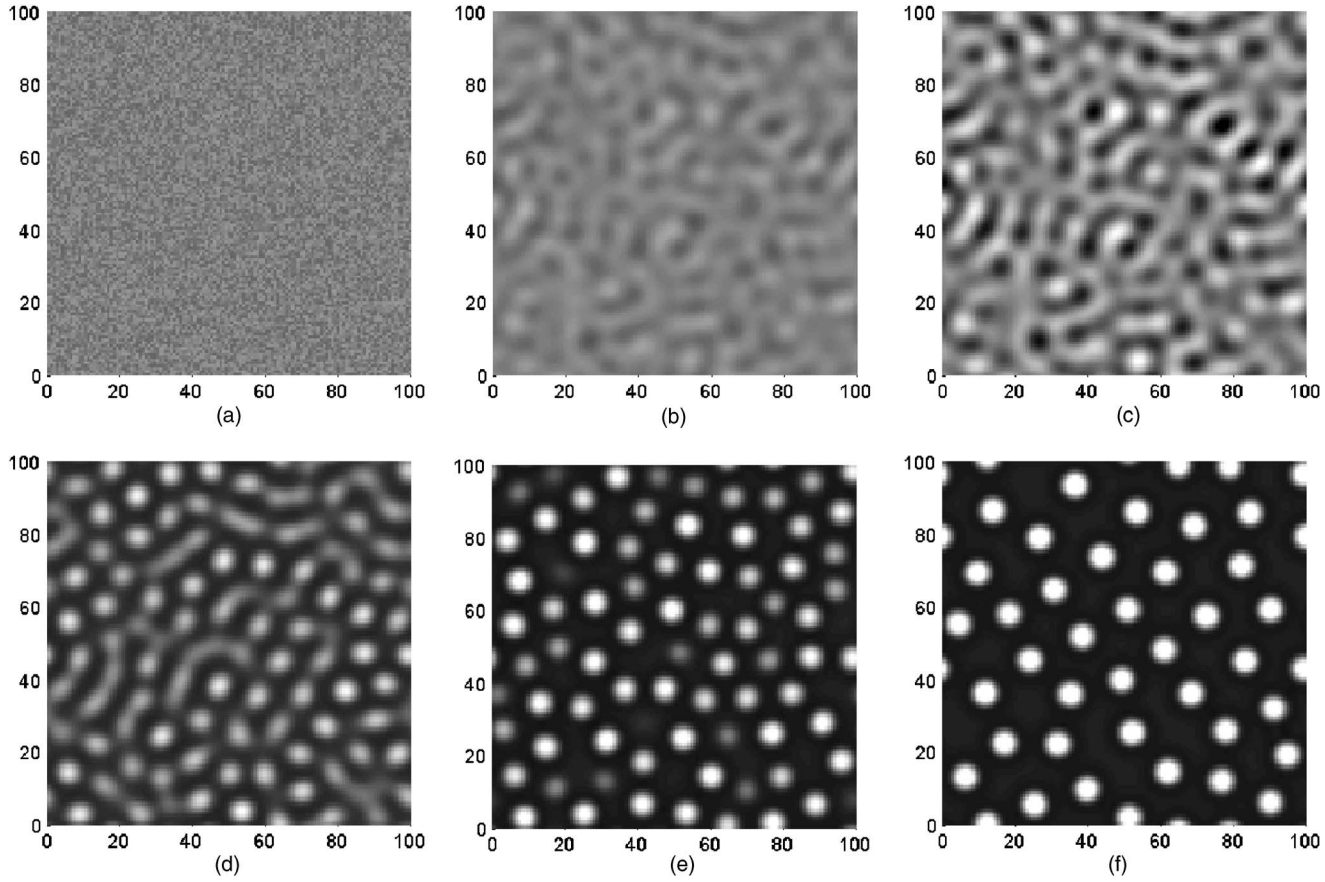

FIG. 8. Three-dimensional simulation of surface evolution based on the nonlinear analysis of both stress and wetting effect. (a)–(f) are gray scale contour plots of the thickness profile $h(x_1,x_2)$, white for crests and dark for troughs. (a) Random perturbation at $t=0$, r.m.s. $=5.77\times10^{-5}$; (b) $t=20$, r.m.s. $=2.07\times10^{-5}$; (c) $t=50$, r.m.s. $=6.27\times10^{-5}$; (d) $t=220$, r.m.s. $=4.86\times10^{-2}$; (e) $t=500$, r.m.s. $=9.11\times10^{-2}$; (f) $t=5000$, r.m.s. $=1.18\times10^{-1}$.

growth rate for the linear and nonlinear equations. The growth rate corresponds well with the fastest growing mode predicted by the linear analysis ($s=0.105$ for $\lambda_m=\frac{8}{3}\pi L$). While the surface evolves self-similarly by the linear equation (Fig. 3), the nonlinear stress field leads to blow-up of the surface roughness when it develops deep pitlike grooves as shown in Fig. 5. Including the wetting effect leads to a slower growth rate at the initial stage ($s=0.042$). Again, the growth rate agrees well with that of the fastest growing mode predicted by the linear analysis (Fig. 6). After about $t=200$, the surface roughness saturates. While coarsening of the island array continues for a much longer time, the r.m.s. surface roughness does not change significantly after $t=500$, which can be understood as a result of the competition between roughening due to the growth of the island height and flattening due to the decrease of the island number density. Also of interest is the combination of the nonlinear wetting potential and the linear stress analysis in the evolution equation. While not presented here, it is found that the solution typically blows up and develops whiskerlike morphology, in contrast to the "steady state" predicted by Tekalign and Spencer.[25] However, the "steady state" was obtained from numerical simulations starting from one period of a sinusoidal perturbation, in which case no coarsening can occur. In our simulations, with a random initial perturbation over a large area, blow-up occurs shortly after coarsening begins, similar to those reported by Spencer *et al.*[23] and Golovin *et al.*[24] Therefore, both the nonlinear stress field and the wet-

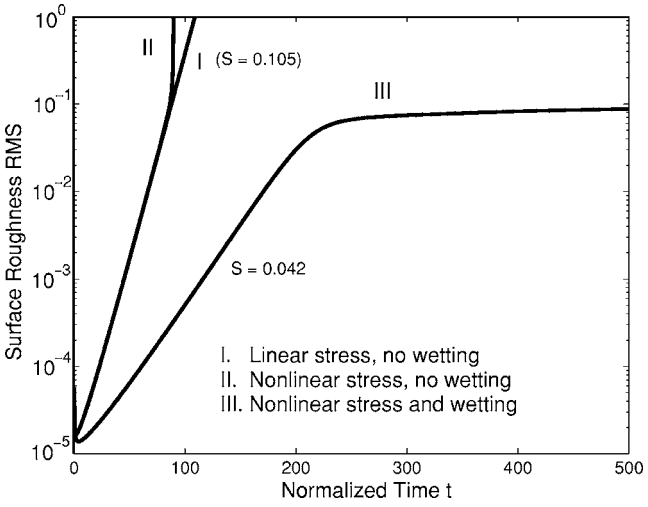

FIG. 9. Comparison of the evolution of surface roughness from three-dimensional simulations using the linear equation (I), the nonlinear equation with no wetting (II), and the nonlinear equation with wetting (III).

ting effect must be included in studying long-time dynamics of surface evolution.

V. CONCLUDING REMARKS

In summary, we have developed a nonlinear evolution equation with a second-order approximation for the stress field and a nonlinear wetting potential for the interface effect. The equation is solved numerically by a spectral method in both two-dimensional (2D) and three-dimensional configurations. In absence of the interface effect, the nonlinear stress field leads to a "blow-up" solution with cracklike grooving in 2D and circular pitlike morphology in 3D. The blow-up is suppressed by the wetting effect for thin films, leading to formation of an array of islands. Subsequent coarsening and stabilization are observed in the simulations. It is thus concluded that the interplay between the nonlinear stress field and the interfacial wetting has a profound effect on the dynamics of surface evolution that may lead to organization of self-assembled islands or quantum dots.

ACKNOWLEDGMENTS

The authors gratefully acknowledge funding of this work by the Department of Energy through Grant No. DE-FG02-05ER46230. Discussions with D. J. Srolovitz of Princeton University and Z. Suo of Harvard University were very helpful.

APPENDIX

For a semi-infinite solid subjected to surface tractions σ_{3j} $(j=1,2,3)$, the displacement at the same surface can be obtained analytically in the Fourier space

$$\hat{u}_i = C_{ij}\hat{\sigma}_{3j}, \tag{A1}$$

where $\hat{u}_i$ and $\hat{\sigma}_{3j}$ are the two-dimensional Fourier transforms of the displacement and the traction, respectively, and

$$[C_{ij}] = \frac{2(1+\nu)}{Ek^3}\begin{bmatrix} (1-\nu)k^2+\nu k_2^2 & -\nu k_1 k_2 & -\frac{1-2\nu}{2}ik_1k \\ -\nu k_1 k_2 & (1-\nu)k^2+\nu k_1^2 & -\frac{1-2\nu}{2}ik_2k \\ \frac{1-2\nu}{2}ik_1k & \frac{1-2\nu}{2}ik_2k & (1-\nu)k^2 \end{bmatrix}. \tag{A2}$$

Here E is Young's modulus of the solid, ν the Poisson's ratio, k_1 and k_2 are components of the wave vector in the Fourier space, and $k^2=k_1^2+k_2^2$. The solution is essentially a combination of the integral solutions for the classical Cerruti and Boussinesq's problems in elasticity.[41]

[1] R. J. Asaro and W. A. Tiller, Metall. Trans. **3**, 1789 (1972).
[2] M. A. Grinfeld, Sov. Phys. Dokl. **31**, 831 (1986).
[3] D. J. Srolovitz, Acta Metall. **37**, 621 (1989).
[4] W. H. Yang and D. J. Srolovitz, Phys. Rev. Lett. **71**, 1593 (1993).
[5] W. H. Yang and D. J. Srolovitz, J. Mech. Phys. Solids **42**, 1551 (1994).
[6] C.-H. Chiu and H. Gao, Int. J. Solids Struct. **30**, 2983 (1993).
[7] B. J. Spencer and D. I. Meiron, Acta Metall. Mater. **42**, 3629 (1994).
[8] Y. Xiang and W. E, J. Appl. Phys. **91**, 9414 (2002).
[9] R. H. Torii and S. Balibar, J. Low Temp. Phys. **89**, 391 (1992).
[10] J. Berrehar, C. Caroli, C. Lapersonne-Meyer, and M. Schott, Phys. Rev. B **46**, 13487 (1993).
[11] L. B. Freund and S. Suresh, *Thin Film Materials: Stress, Defect Formation and Surface Evolution* (Cambridge University Press, Cambridge, 2004).
[12] B. J. Spencer, P. W. Voorhees, and S. H. Davis, Phys. Rev. Lett. **67**, 3696 (1991).
[13] L. B. Freund and F. Jonsdottir, J. Mech. Phys. Solids **41**, 1245 (1993).
[14] H. Liu and R. Huang, J. Appl. Phys. **97**, 113537 (2005).
[15] D. J. Eaglesham and M. Cerullo, Phys. Rev. Lett. **64**, 1943 (1990).
[16] C. S. Ozkan, W. D. Nix, and H. Gao, Appl. Phys. Lett. **70**, 2247 (1997).
[17] H. Gao and W. D. Nix, Annu. Rev. Mater. Sci. **29**, 173 (1999).
[18] M. Coll, J. Gazquez, A. Pomar, T. Puig, F. Sandiumenge, and X. Obradors, Phys. Rev. B **73**, 075420 (2006).
[19] J. Tersoff and F. K. LeGoues, Phys. Rev. Lett. **72**, 3570 (1994).
[20] Y. W. Zhang and A. F. Bower, J. Mech. Phys. Solids **47**, 2273 (1999).
[21] P. Liu, Y. W. Zhang, and C. Lu, Phys. Rev. B **68**, 035402 (2003).
[22] C.-H. Chiu, Phys. Rev. B **69**, 165413 (2004).
[23] B. J. Spencer, S. H. Davis, and P. W. Voorhees, Phys. Rev. B **47**, 9760 (1993).
[24] A. A. Golovin, S. H. Davis, and P. W. Voorhees, Phys. Rev. E **68**, 056203 (2003).
[25] W. T. Tekalign and B. J. Spencer, J. Appl. Phys. **96**, 5505 (2004).
[26] B. J. Spencer, Phys. Rev. B **59**, 2011 (1999).
[27] R. V. Kukta and L. B. Freund, J. Mech. Phys. Solids **45**, 1835 (1997).
[28] M. Ortiz, E. A. Repetto, and H. Si, J. Mech. Phys. Solids **47**, 697 (1999).
[29] Y. W. Zhang, Phys. Rev. B **61**, 10388 (2000).

[30] V. B. Shenoy and L. B. Freund, J. Mech. Phys. Solids **50**, 1817 (2002).
[31] T. V. Savina, P. W. Voorhees, and S. H. Davis, J. Appl. Phys. **96**, 3127 (2004).
[32] M. Seul and D. Andelman, Science **267**, 476 (1995).
[33] N. Bowden, S. Brittain, A. G. Evans, J. W. Hutchinson, and G. M. Whitesides, Nature (London) **393**, 146 (1998).
[34] P. J. Yoo and H. H. Lee, Phys. Rev. Lett. **91**, 154502 (2003).
[35] W. Lu and Z. Suo, J. Mech. Phys. Solids **49**, 1937 (2001).
[36] Z. Huang, W. Hong, and Z. Suo, Phys. Rev. E **70**, 030601(R) (2004).
[37] Z. Suo and W. Wang, J. Appl. Phys. **76**, 3410 (1994).
[38] J. A. Floro, S. J. Hearne, J. A. Hunter, P. Kotula, E. Chason, S. C. Seel, and C. V. Thompson, J. Appl. Phys. **89**, 4886 (2001).
[39] F. M. Ross, J. Tersoff, and R. M. Tromp, Phys. Rev. Lett. **80**, 984 (1998).
[40] W. Dorsch, H. P. Strunk, H. Wawra, G. Wagner, J. Groenen, and R. Carles, Appl. Phys. Lett. **72**, 179 (1998).
[41] M. H. Saad, *Elasticity: Theory, Applications, and Numerics* (Elsevier Academic Press, Amsterdam, 2005).